J. Plasma Fusion Res. SERIES, Vol. 6 (2004) 60–63

Particle Acceleration Mechanisms in Magnetosonic Shock Waves

OHSAWA Yukiharu
Department of Physics, Nagoya University, Nagoya, 464-8602, Japan
(Received: 9 December 2003 / Accepted: 6 July 2004)

Abstract

Theory and simulations of nonstochastic particle acceleration mechanisms occurring in collisionless shock waves in a magnetized plasma are reviewed. We describe the acceleration mechanisms of hydrogen ions, heavy ions, electrons, nonthermal relativistic ions, and positrons. The first three mechanisms explain the basic properties of solar energetic particles; i.e., prompt acceleration of ions to energies $10^9 \sim 10^{10}$ eV and electrons to $10^7 \sim 10^8$ eV, with elemental compositions of high-energy heavy ions similar to that of the solar corona. For the last two mechanisms, the maximum energies demonstrated by simulations far exceed the level of solar energetic particles.

Keywords:
particle acceleration, collisionless shock wave, particle simulation, hydrogen, heavy ion, electron, positron

1. Introduction

Acceleration of charged particles in laboratory and astrophysical plasmas has been extensively studied by many authors [1-8]. To understand particle acceleration, we need to study collective plasma behavior as well as individual particle motions in a self-consistent manner. Particle simulations are therefore a powerful tool for this research. Indeed, for instance, they have shown that magnetosonic shock waves (or pulses) can accelerate particles with various nonstochastic mechanisms; i.e., hydrogen ions [9-16], heavy ions [17,18], electrons [19,20], nonthermal relativistic ions [20,21], and positrons [23]. The first three mechanisms explain the basis properties of solar energetic particles; prompt acceleration of ions to relativistic energies and electrons to ultrarelativistic energies, with the elemental compositions of energetic heavy ions quite similar to that of the solar corona. On the other hand, in the last two mechanisms (relativistic ions and positrons) particle energies far exceed the level of the solar energetic particles. This paper very briefly reviews the theory and simulation results of these acceleration processes.

2. Ion acceleration

2.1 Hydrogen ions

In a single-ion-species plasma, a magnetosonic shock wave can accelerate some ions by reflection; the reflection occurs owing to the rapid increase in the electric potential or the magnetic field [9-16]. The maximum speed of reflected ions is $v \sim 2Mv_A$, where M is the Alfvén Mach number and v_A is the Alfvén speed. When the electron gyrofrequency is greater than the plasma frequency, $|\Omega_e|/\omega_{pe} \gtrsim 1$, these ions can become relativistic.

In this paper, shock waves are assumed to propagate in the x direction with a speed v_{sh} in an external magnetic field in the (x, z) plane, $\boldsymbol{B}_0 = B_0(\cos\theta, 0, \sin\theta)$. Figure 1 shows ion phase space plots (x, p_x) and (x, p_y), where p_x and p_y are the x and y components of the momentum $\boldsymbol{p}$, respectively. Many ions are accelerated to relativistic energies by a shock wave (the shock front is at $x/\Delta_g \simeq 1500$ at this moment, where Δ_g is the grid spacing). This result was obtained by a relativistic, electromagnetic particle simulation with full ion and electron dynamics [12]. In the laboratory frame, the quantities $B_z - B_{z0}$, E_y, and electric potential ϕ have similar profiles. (In the wave frame, E_y is constant.) The simulation parameters for Fig. 1 are as follows: $m_i/m_e = 100$, $|\Omega_e|/\omega_{pe} = 3$, $\theta = 90^\circ$, and $v_A/c = 0.3$. The observed shock

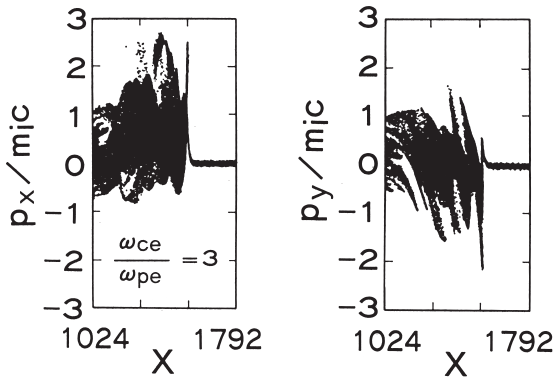

Fig. 1 Phase space plots of ions accelerated to relativistic energies by a shock wave.

Corresponding author's e-mail: ohsawa@phys.nagoya-u.ac.jp

speed is $v_{sh} = 2.7 v_A$.

In this example, the ions are strongly accelerated once; both p_x and p_y monotonically increase to their maximum values after the reflection. It was suggested [10], however, that multiple reflection of an ion can occur at a shock front. This can take place when v_x is very close to v_{sh} when the ion encounters the shock wave. If the thermal speed is much lower than v_{sh}, as shown in Fig. 1, the multiple reflection will rarely happen [15]., i.e., the number of such particles will be small in a low beta plasma.

2.2 Heavy ions

In a plasma containing multiple ion species with the hydrogen being the major component, a shock wave accelerates all the heavy ions [17]. (Some hydrogen ions are accelerated by the reflection, as discussed in Sec. **2.1**.) The maximum speeds of the heavy ions are nearly the same, independent of particle species,

$$v \sim \left(\frac{B_m - B_0}{B_m + B_0} \right) v_{sh}, \tag{1}$$

where B_m is the peak value of B.

If large-amplitude magnetosonic pulses are excited in the solar corona, therefore, the elemental compositions of high-energy heavy ions should be quite similar to that of the solar corona [3]. If they are excited in coronal magnetic tubes, where the magnetic fields are strong, the particle energies would be quite high.

This acceleration becomes weak as the wave amplitude is decreased. It does not vanish, however, as long as the amplitude is finite. Hence, magnetosonic solitary waves are damped even if they propagate perpendicular to a magnetic field. Aside from the particle acceleration, the presence of multiple ion species introduces various interesting phenomena in the wave propagation (see refs. [24,25] and references therein).

3. Electron acceleration to ultrarelativistic energies

If some electrons are reflected near the end of the main pulse of a shock wave, they can be accelerated to ultrarelativistic energies in the shock region [19, 20]. Here, we theoretically describe this, considering particle trajectories.

From the relativistic equation of motion for an electron,

$$m_e \frac{\mathrm{d}(\gamma \boldsymbol{v})}{\mathrm{d}t} = -e \left(\boldsymbol{E} + \frac{\boldsymbol{v} \times \boldsymbol{B}}{c} \right), \tag{2}$$

where γ is the Lorentz factor, we have the energy conservation equation in the wave frame,

$$m_e c^2 (\gamma - \gamma_0) = e(\phi - \phi_0) - e E_{y0} \int v_y \, \mathrm{d}t. \tag{3}$$

Here, we have used the relations $E_y = E_{y0}$ (constant) and $E_z = 0$, which hold in the wave frame. We show in Fig. 2 a schematic diagram of guiding-center orbit projected on the

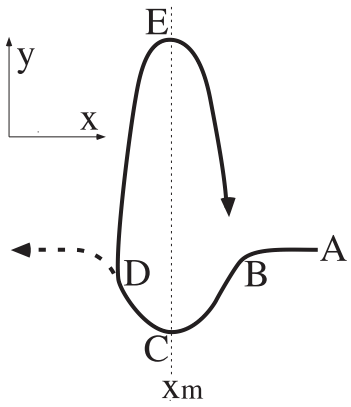

Fig. 2 Electron guiding center orbit projected on the (x, y) plane.

(x, y) plane; some electrons are reflected at point D. Point C and point E are on the peak of the potential ϕ; hence, $x_C = x_E = x_m$, where x_m designates the x position at which ϕ and B_z take their maximum values. The electric field E_x is positive in the region $x > x_m$ and is negative in $x < x_m$. Substituting the guiding-center velocity

$$v_{gx} = \frac{c E_{y0} B_z}{B^2} + v_{\parallel} \frac{B_{x0}}{B}, \tag{4}$$

$$v_{gy} = -\frac{c E_x B_z}{B^2} + v_{\parallel} \frac{B_y}{B}, \tag{5}$$

in eq. (3), we find the increase in the kinetic energy from point B to point C as

$$\begin{aligned} K_{BC} = {} & e(\phi_C - \phi_B) \\ & + e E_{y0} \int_B^C \mathrm{d}x \, E_x / [E_{y0} + (v_{\parallel}/c)(B B_{x0}/B_z)] \\ & - e E_{y0} \int_B^C \mathrm{d}t \, v_{\parallel} B_y / B. \end{aligned} \tag{6}$$

The first term on the right-hand side shows the energy change by the potential difference. The second and third terms represent the work done by the constant electric field E_{y0}. We have similar expressions for K_{CD} and K_{DE}. The energy increase from point B to point E is given by $K_{BE} = K_{BC} + K_{CD} + K_{DE}$. The magnitudes of K_{BC} and K_{CD} are quite small because the changes in the kinetic energy due to the electric potential ϕ and due to E_{y0} almost cancel [19]. In moving from points D to E, however, electrons gain energy from both ϕ and E_{y0}, which makes K_{DE} quite large. Hence, $K_{BE} \simeq K_{DE}$. Now, assuming that, shortly after the reflection, the electrons have relativistic velocities $v_{\parallel} \sim c$ and that $B \sim B_z \gg B_y$ (B_y is small in the simulations), we obtain the electron energy at point E as

$$K_{BE} = \frac{e\phi_E}{1 - (v_{sh}/c)(B_{z0}/B_{x0})}. \tag{7}$$

This indicates that K_{BE} can have extremely great values when the denominator is close to zero. This condition is identical to the relation $v_{gx} \sim 0$. In this case, it takes a long

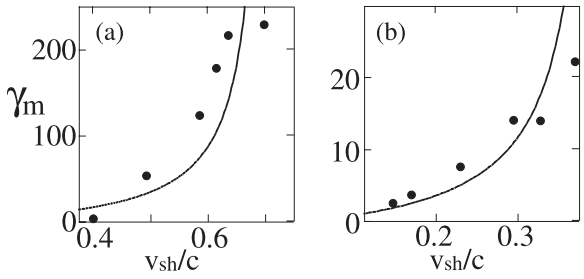

Fig. 3 The maximum electron energy as a function of v_{sh}. The solid lines and dots show theory and simulation results, respectively. Here, $|\Omega_e|/\omega_{pe} = 3$ and $\theta = 45°$ in (a), while $|\Omega_e|/\omega_{pe} = 1$ and $\theta = 66°$ in (b).

time to move from point D to E, during which the particle traverses a long distance in the y direction, gaining a great amount of energy from E_{y0}. The magnitude of the potential in the wave frame is given as [26]

$$e\phi_E = m_i v_A^2 \gamma_{sh}\left[\sin^2\theta + \frac{\sin\theta\cos\theta}{\gamma_{sh}(1+\gamma_{sh}^2\tan^2\theta)^{1/2}}\right] \times\left[\left(1+\frac{2v_{sh}^2}{v_A^2\sin^2\theta}\right)^{1/2}-1\right], \quad (8)$$

where $\gamma_{sh} = (1-v_{sh}^2/c^2)^{-1/2}$. Figure 3 shows the maximum electron energy as a function of v_{sh}. The solid line and dots represent the theory and simulation results, respectively.

4. Acceleration of nonthermal relativistic particles

In the previous three mechanisms, particles are accelerated from thermal to high energies. In this section, we discuss a mechanism accelerating nonthermal energetic particles to much higher energies.

When

$$v_{sh} \sim c\cos\theta, \quad (9)$$

is satisfied,the interaction time between relativistic particles and wave fields can become significantly long [21,22,23]. Indeed, since the time-averaged particle velocity in the x direction, $\langle v_x \rangle$, is limited by $c\cos\theta$, particles cannot quickly outrun the wave if (9) holds. It was shown [21,22] that by virtue of this effect, nonthermal, fast ions with $\gamma \sim 1$ can be accelerated to ultrarelativistic energies with $\gamma > 100$ by an oblique shock wave satisfying eq. (9) (see Fig. 4, where γ grows from 4 to 160).

Relativistic ions have gyration speeds comparable to or faster than v_{sh} and gyroradii much larger than the width of the shock transition region. In association with the gyromotion, thus, these particles can move back and forth between the pulse and upstream regions [27,28,29]; when they are in the shock region, they gain energy from the transverse electric field E_y, because their motions are nearly parallel to E_y there. Hence, while they move with the wave, their energies increase stepwise, with each energy jump given by

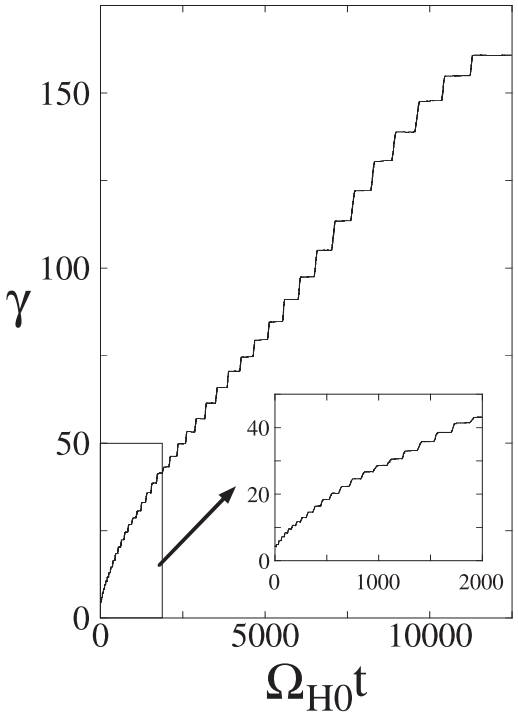

Fig. 4 Stepwise increase in γ of a relativistic ion incessantly accelerated by an oblique shock wave. Here, Ω_{H0} is the nonrelativistic hydrogen gyrofrequency in the upstream region.

$$\delta\gamma = \frac{2q_i p_{1\perp} E_{1y}}{m_i^2 c^2 \Omega_{i1}} \sin\left[\frac{\Omega_{i1}(t_{out}-t_{in})}{2\gamma}\right]. \quad (10)$$

Here, q_i is the ion charge, and Ω_i is the nonrelativistic ion gyrofrequency. The subscript 1 refers to quantities in the strong-field region; $p_{1\perp}$ is the momentum perpendicular to the magnetic field. The energy increase rate averaged over the gyroperiod [22] is

$$\frac{d\gamma}{dt} = \frac{g_{01}}{\pi}\frac{v_{1\perp}v_{sh}}{c^2}\Omega_{i01}, \quad (11)$$

where g_{01} is a numerical factor smaller than unity,

$$g_{01} = \left(1-\frac{B_{z0}}{B_{z1}}\right)\left(1-\frac{B_{x0}^2}{2B_{z1}^2}\right)\sin\left[\frac{\Omega_{i1}(t_{out}-t_{in})}{2\gamma}\right]. \quad (12)$$

5. Positron acceleration

Strong positron acceleration in a shock wave with eq. (9) has also been demonstrated with particle simulations [23]. Although the electric field parallel to the magnetic field, $E_\parallel$, is quite weak in magnetohydrodynamic waves, positrons can be reflected by $E_\parallel$ because the positron mass is much smaller than ion masses. They gain a large amount of energy while moving with the wave. (The reflection of hydrogen ions is across $\boldsymbol{B}$.)

If γ is large, a slight change in the speed can lead to a great change in γ. Using this fact,

$$v\,d\gamma/dt \gg \gamma\,dv/dt, \quad (13)$$

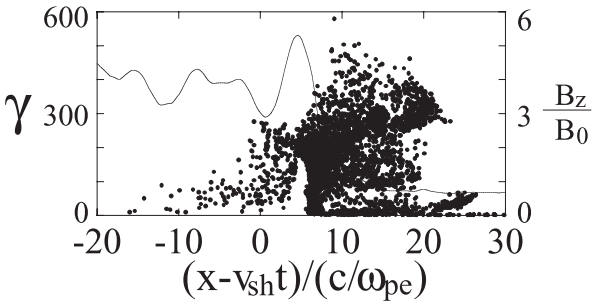

Fig. 5 Positron phase space plots (x, γ). The solid line shows the profile of B_z.

one can theoretically find particle motions where the zeroth-order velocity is nearly parallel to the external magnetic field. This theory explains the positron acceleration observed in particle simulations.

Figure 5 shows phase space plots of positrons accelerated by a shock wave with $v_{sh}=2.4v_A$ in a plasma with $v_A/c=0.2$ and $\theta=61°$. The plasma contains positrons as well as electrons and ions with the positron-to-electron density ratio $n_p/n_e=1/50$. Unlike the above energetic ions, these positrons are in the shock transition region during the acceleration process.

6. Summary

We have very briefly reviewed five different particle acceleration mechanisms caused by magnetosonic shock waves. They are demonstrated by simulations and are explained by a coherent theory. Even though we have not described the nonlinear wave theory [30-35] or simulation methods, they play an essential role in the understanding of particle acceleration.The development of plasma physics is needed to resolve the mystery of cosmic ray acceleration.

Acknowledgements

The author is grateful to Dr. M. Toida, Dr. N. Bessho, Dr. S. Irie, Mr. S. Usami, and Mr. H. Hasegawa. This paper is based on the collaboration with them.

References

[1] D.J. Forrest and E.L. Chupp, Nature (London) **305**, 291 (1983).
[2] E.L. Chupp *et al*., Astrophys. J. **318**, 913 (1987).
[3] J.P. Meyer, Astrophys. J. Suppl. **57**, 151 (1985); *ibid*. **57**, 173 (1985).
[4] K. Koyama *et al*., Nature (London) **378**, 255 (1995).
[5] T. Tanimori *et al*., Astrophys. J. Lett. **497**, L25 (1998).
[6] T. Tajima and J.M. Dawson, Phys. Rev. Lett. **43**, 267 (1979).
[7] T. Katsouleas and J.M. Dawson, Phys. Rev. Lett. **51**, 392 (1983).
[8] C. Joshi and T. Katsouleas, Physics Today **56**, No. 6, 47 (1994).
[9] D. Biskamp and H.Welter, Nucl. Fusion **12**, 663 (1972).
[10] R.Z. Sagdeev and V.D. Shapiro, Zh. Eksp. Teor. Fiz. Pis'ma Red. **17**, 387 (1973) [JETP Lett. **17**, 279 (1973)].
[11] D.W. Forslund, K.B. Quest, J.U. Brackbill and K. Lee, J. Geophys. Res [Oceans] **89**, 2142 (1984).
[12] Y. Ohsawa, Phys. Fluids **28**, 2130 (1985).
[13] B. Lembege and J.M. Dawson, Phys. Fluids **B1**, 1001 (1989).
[14] R.L. Tokar, S.P. Gary and K.B. Quest, Phys. Fluids **30**, 2569 (1987).
[15] Y. Ohsawa, J. Phys. Soc. Jpn. **59**, 2782 (1990).
[16] T. Kawashima, S. Miyahara and Y. Ohsawa, J. Phys. Soc. Jpn. **72**, 1664 (2003).
[17] M. Toida and Y. Ohsawa, Sol. Phys. **171**, 161 (1997).
[18] D. Dogen, M. Toida and Y. Ohsawa, Phys. Plasmas **5**, 1298 (1998).
[19] N. Bessho and Y. Ohsawa, Phys. Plasmas **6**, 3076 (1999).
[20] N. Bessho and Y. Ohsawa, Phys. Plasmas **9**, 979 (2002).
[21] S. Usami, H. Hasegawa and Y. Ohsawa, Phys. Plasmas **8**, 2666 (2001).
[22] S. Usami and Y. Ohsawa, Phys. Plasmas **9**, 1069 (2002).
[23] H. Hasegawa, S. Usami and Y. Ohsawa, Phys. Plasmas **10**, 3455 (2003).
[24] M. Toida, Y. Ohsawa and T. Jyounouchi, Phys. Plasmas **2**, 3329 (1995).
[25] S. Irie and Y. Ohsawa, Phys. Plasmas **10**, 1253 (2003).
[26] S. Miyahara, T. Kawashima and Y. Ohsawa, Phys. Plasmas **10**, 98 (2003).
[27] K. Maruyama, N. Bessho and Y. Ohsawa, Phys. Plasmas **5**, 3257 (1998).
[28] T. Masaki, H. Hasegawa and Y. Ohsawa, Phys. Plasmas **7**, 529 (2000).
[29] R.B. Decker, Space Sci. Rev. **48**, 195 (1988).
[30] J.H. Adlam and J.E. Allen, Philos. Mag. Suppl. **3**, 448 (1958).
[31] L. Davis, R. Lüst and A. Schlüter, Z. Naturforsch. A **13**, 916 (1958).
[32] C.S. Gardner and G.K. Morikawa, Commun. Pure Appl. Math. **18**, 35 (1965).
[33] T. Kakutani, H. Ono, T. Taniuti and C.C. Wei, J. Phys. Soc. Jpn. **24**, 1159 (1968).
[34] Y. Ohsawa, Phys. Fluids **29**, 1844 (1986).
[35] Y. Ohsawa, Phys. Fluids **29**, 2474 (1986).